Reduced Graphene Oxide and Porphyrin. An Interactive Affair in 2-D

Aleksandra Wojcik[§] and Prashant V. Kamat*

Radiation Laboratory and Department of Chemistry and Biochemistry, University of Notre Dame, Notre Dame, Indiana 46556, United States. [§]On leave from the Faculty of Chemistry, Adam Mickiewicz University, Poznan, Poland.

ARTICLE

ABSTRACT Photoexcited cationic 5,10,15,20-tetrakis(1-methyl-4-pyridinio)porphyrin tetra(*p*-toluenesulfonate) (TMPyP) undergoes charge-transfer interaction with chemically reduced graphene oxide (RGO). Formation of the ground-state TMPyP—RGO complex in solution is marked by the red-shift of the porphyrin absorption band. This complexation was analyzed by Benesi—Hildebrand plot. Porphyrin fluorescence lifetime reduced from 5 to 1 ns upon complexation with RGO, indicating excited-state interaction between singlet excited porphyrin and RGO. Femtosecond transient absorption measurements carried out with TMPyP adsorbed on RGO film revealed fast decay of the singlet excited state, followed by the formation of a longer-living product with an absorption maximum around 515 nm indicating the formation of a porphyrin radical cation. The ability of TMPyP—RGO to undergo photoinduced charge separation was further confirmed from the photoelectrochemical measurements. TMPyP—RGO coated conducting glass electrodes are capable of generating photocurrent under visible excitation. These results are indicative of the electron transfer between photoexcited porphyrin and RGO. The role of graphene in accepting and shuttling electrons in light-harvesting assemblies is discussed.

KEYWORDS: graphene oxide · porphyrin · 2-D interactions · electron transfer · photocurrent

Graphene is a two-dimensional (2-D) nanomaterial consisting of sp^2-hybridized carbon atoms forming a one-atom thick honeycomb lattice. Owing to its unique structure and electronic properties, it has drawn the attention of scientists in recent years.[1−5] Solution processable graphene oxide sheets are readily prepared by oxidizing graphite according to the Hummers method.[6] The exfoliated graphene oxide sheets (GO) are suspendable in polar solvents, and they can be reduced to produce reduced graphene oxide (RGO).[7−10] The thermal, chemical,[11] sonochemical,[12] microwave,[13−15] photocatalytic,[16−18] or electrochemical[19] treatment used to reduce GO can only partially restore aromatic sp^2 structure of graphene. By varying the degree of GO reduction, it is possible to tune the properties of RGO.[20−23]

Since the reduced graphene oxide exhibits many physical properties similar to that of graphene, they are being considered in electronic, sensor, and catalytic applications.[24−31] Attempts to use blends of functionalized graphene and poly(3-hexylthiophene) as an active layer in a polymer solar cell resulted in a power conversion efficiency of 1.4%.[32,33] Incorporation of graphene sheets into TiO_2 nanoparticle films used as photoanodes in dye-sensitized solar cells gave five times the power conversion efficiencies than those obtained with TiO_2 nanoparticle films without carbon sheets.[34] Importance of graphene was also shown in field-effect transistors,[35,36] sensors,[37,38] and catalysis.[30] Improved photocatalytic performance has also been reported for TiO_2—RGO composite films.[39]

Another interesting aspect is the noncovalent functionalization of graphene, with planar organic molecules *via* π−π stacking, van der Waals, and/or electrostatic forces. Interaction with electron-withdrawing or -donating aromatic molecules, such as nitrobenzene and aniline, results in the doping of graphene.[40] Positively charged aromatic dyes, such as methylene green, can increase the dispersity of graphene oxide.[41] Interaction of RGO with pyrenebutyrate, rhodamine 6G, porphyrin, and thiophene derivatives are often marked by fluorescence quenching of organic molecules.[42−46]

Numerous reports have appeared discussing photoinduced charge separation in porphyrin single-wall carbon nanotubes[47−50] and porphyrin−fullerenes[51−54] supramolecular assemblies. Although fluorescence quenching provides a fingerprint for establishing excited-state interaction in graphene-based systems, this technique alone cannot establish the mechanism of the quenching process. For example, in the case of porphyrin

***Address correspondence to pkamat@nd.edu.**

Received for review August 27, 2010 and accepted October 14, 2010.

Published online October 28, 2010. 10.1021/nn102185q

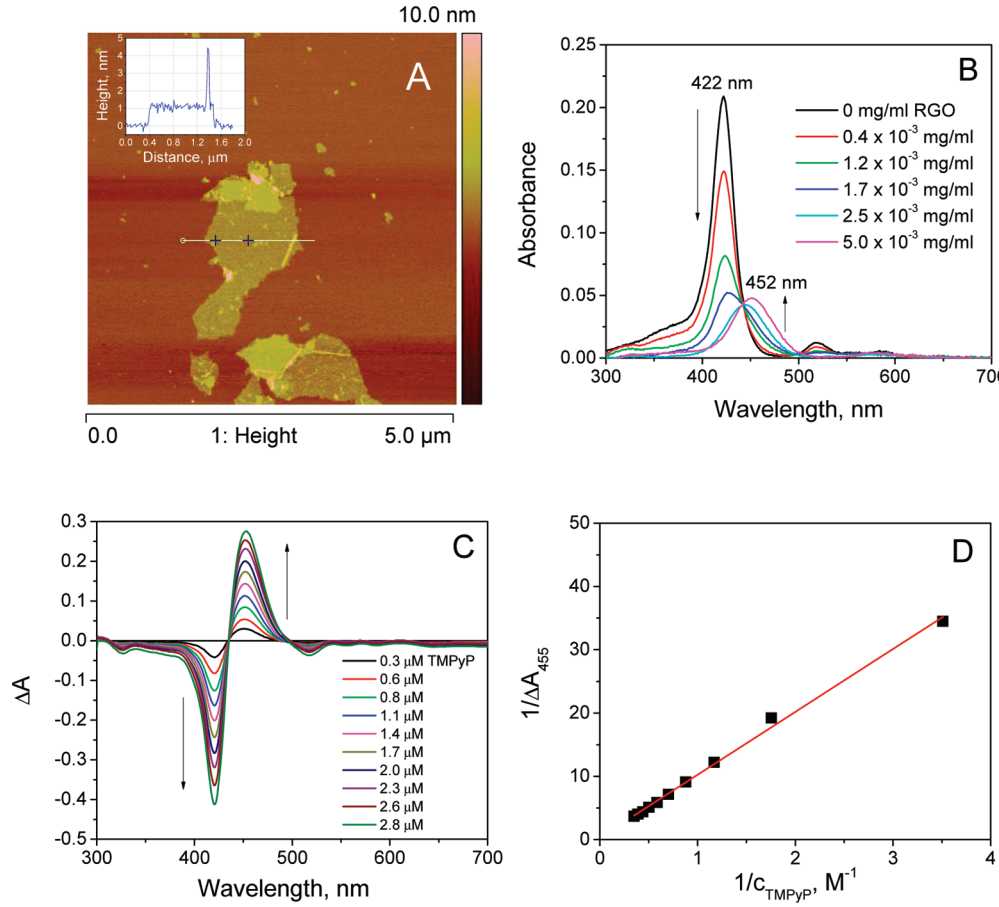

Figure 1. (A) AFM image of single-sheet reduced graphene oxide captured on mica substrate together with depth profile along the line of interest on RGO sheet. (B) Absorption spectra recorded during addition of 0.25 mg/mL aqueous suspension of RGO (0−60 µL) to 1 µM TMPyP in H_2O (3 mL). All spectra corrected for the RGO absorption. (C) Absorption spectra recorded with two-beam spectrophotometer during addition of aqueous solution of 170 µM TMPyP (5−50 µL) to 0.05 mg/mL RGO in H_2O (3 mL); $\Delta A = A - A_0$, where A corresponds to the absorbance of the sample with TMPyP and RGO, and A_0 corresponds to the absorbance of the TMPyP alone. (D) Benesi−Hildebrand plot showing linear dependence of the inverse of ΔA at 455 nm on the inverse of the TMPyP concentration. Black squares are the experimental points, and the red line is the linear fit.

linked to graphene *via* an amide bond, intramolecular energy transfer is postulated to explain the fluorescence quenching.[55] As shown in our earlier studies with TiO_2−RGO systems, the 2-D graphene sheets have the capability to accept and shuttle electrons.[30,39] The obvious question is whether such a property would be useful for manipulating electron transfer between the excited sensitizer and RGO. We have now employed a cationic 5,10,15,20-tetrakis(1-methyl-4-pyridinio)porphyrin tetra(*p*-toluenesulfonate) (TMPyP) sensitizer to probe the ground-state interaction as well as the mechanism of excited-state deactivation on RGO surfaces.

RESULTS AND DISCUSSION

Characterization of the RGO(TMPyP)$_n$ Complex in Solution. Reduced graphene oxide (RGO) sheets suspended in water usually exist as individual sheets as well as a few (2−4) stacked sheets. The presence of RGO sheets in the suspension was confirmed by atomic force microscopy (AFM). The AFM image in Figure 1A shows a single RGO sheet captured from the suspension on a mica substrate. Detailed characterization of the RGO sheets imaged with AFM can be found elsewhere.[16,56,57]

TMPyP is a water-soluble tetracationic porphyrin, with N-methylated pyridine substituents which are nearly perpendicular to the plane of the porphyrin (Chart 1). Typically, the planar structure of the dye facilitates interaction with carbon nanostructures, such as carbon nanotubes.[58,59] In order to examine the ground-state interaction between porphyrin and RGO, we recorded absorption spectra at different concentrations of RGO.

The absorption spectra of TMPyP recorded with the addition of a RGO suspension are shown in Figure 1B. After each injection of RGO suspension, the solution was allowed to stand for 15 min so that the system attains equilibrium. In the absence of RGO, a Soret band of TMPyP appears at *ca.* 422 nm, together with four less intense Q-bands at *ca.* 520, 559, 587, and 643 nm.[60]

In the presence of RGO, maximum of the Soret band red-shifts from 422 (ε_{422} = 201 600 M^{-1} cm^{-1}) to 452 nm, with an isosbestic point at 442 nm. Spectra pre-

sented in Figure 1B were corrected for the corresponding absorption of RGO. The observed shift in the absorption band is in good agreement with the RGO-induced red-shift of the porphyrin Soret band, as reported by Xu et al.[61] Such a strong shift of the absorption maximum was attributed to the flattening of the TMPyP molecule driven by $\pi-\pi$ stacking and electrostatic interactions between the porphyrin moiety and the RGO sheet. AFM images of the RGO−TMPyP complex confirmed a monolayer coverage of graphene surface by porphyrin molecules and a lack of 2-D ordering of TMPyP on RGO surface. These results are in agreement with earlier studies in which TMPyP molecules were adsorbed onto laponite or mica sheets.[62,63] Rotation of the N-methylated pyridine substituents to the same plane as the porphyrin ring results in the extension of the π conjugation and the batochromic shift of the Soret band. Although protonation of the adsorbed TMPyP molecules could also lead to spectral shifts,[64,65] we consider such a possibility unlikely because of the slight basicity of the dispersed medium (pH = 7.5−8.5).[65] Under such experimental conditions TMPyP exists as a free base, bearing four positive charges at its N-methylated pyridine substituents.

We further analyzed the interaction between TMPyP and RGO (eq 1) using the Benesi−Hildebrand method[66]

$$\mathrm{RGO} + n\mathrm{TMPyP} \rightleftarrows \mathrm{RGO(TMPyP)}_n \qquad (1)$$

where n denotes the average number of TMPyP molecules that interact with a single RGO sheet. By employing one of the reagents (TMPyP) in excess and varying its concentration, we can shift the equilibrium to the right and monitor the formation of the associated complex ($\mathrm{RGO(TMPyP)}_n$). The absorption spectrum of the equilibrium mixture (*viz.*, RGO and TMPyP mixed suspension) represents superposition of the absorption spectrum of the associated complex and the free reagents present in the suspension. A quartz cuvette with aqueous suspension of RGO in the sample beam and another cuvette with pure water in the reference beam were introduced in the dual beam spectrophotometer. The same amounts of concentrated TMPyP solution in known increments were added to cells in both compartments, and the suspension was allowed to equilibrate. Since the absorption spectra were recorded with TMPyP (without RGO) as reference, it allowed us to directly record the difference absorption spectra (Figure 1C). With an increasing concentration of TMPyP, we observed an increased contribution of the $\mathrm{RGO(TMPyP)}_n$ complex to the absorption and the depletion of the absorption of TMPyP. The appearance of difference absorbance maximum at 455 nm and the simultaneous bleaching of the porphyrin band in Figure 1C highlight the difference absorption features of the RGO−TMPyP complex.

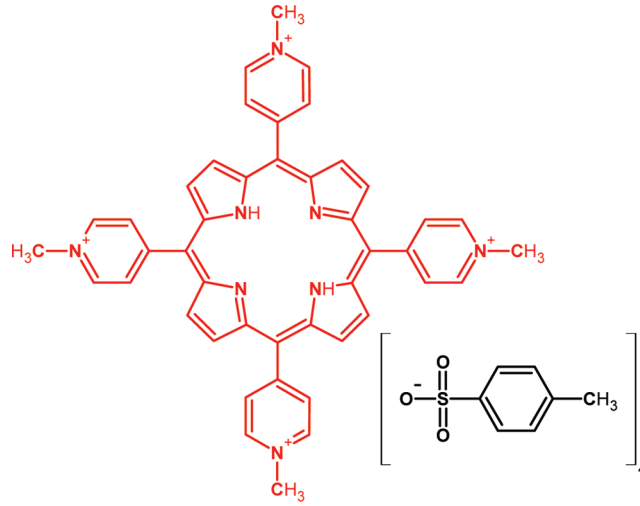

Chart 1. Structure of TMPyP.

The spectra in Figure 1C were further analyzed using the Benesi−Hildebrand expression (eq 2):[66]

$$1/\Delta A_{455} = 1/(1*\varepsilon_{455}*K_a*c_{\mathrm{RGO}}*c_{\mathrm{TMPyP}}) + 1/1*\varepsilon_{455}*c_{\mathrm{RGO}} \qquad (2)$$

where K_a denotes the apparent association constant, ε is the molar absorption coefficient of TMPyP adsorbed on RGO, and c_{RGO} is the concentration of RGO. Inverse of the difference absorbance at 455 nm ($1/\Delta A_{455}$) was plotted versus inverse of the TMPyP concentration ($1/c_{\mathrm{TMPyP}}$). The linearity of the plot in Figure 1D confirms the complex formation between RGO and TMPyP (eq 1). Using the slope and the intercept of the linear fit we obtained the apparent association constant as 3.1×10^4 M^{-1}. The value of K_a should be treated with caution since multiple binding sites for TMPyP molecules at a single RGO sheet and various sizes and degrees of aggregation of reduced graphene oxide sheets are likely to interfere with the determination of the absolute value. However, the large apparent value of K_a shows that the complexation between TMPyP and RGO sheets is rather strong and that it can be achieved in relatively dilute solutions.

RGO-Induced Fluorescence Quenching in Solution. To probe the interaction between the excited-state of TMPyP and RGO in solution, fluorescence spectra of TMPyP at different RGO concentrations were recorded. As shown in Figure 2A, a decrease in the TMPyP fluorescence intensity is seen with increasing RGO concentration, thus confirming a strong interaction between the two.

TMPyP has a broad emission comprising of two unresolved Q(0,0) and Q(0,1) bands at *ca.* 675 and 705 nm, respectively.[67] Vergeldt *et al.* postulated that coalescence of the Q-bands is caused by the mixing of the first excited-state S_1 of the porphyrin and the charge-transfer (CT) state in which an electron is transferred from the porphyrin macrocycle to the pyridinium substituent. For coplanar orientation of the pyridinium groups and the porphyrin macrocycle, electronic cou-

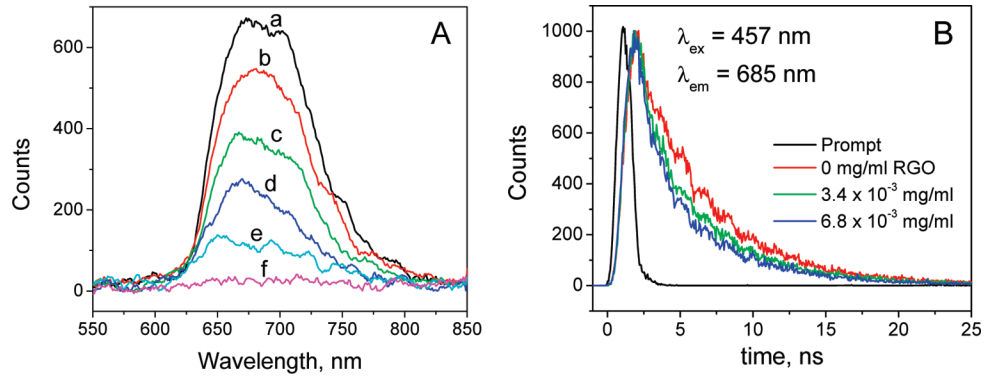

Figure 2. (A) Quenching of the fluorescence of 1 μM TMPyP in H_2O (3 mL) recorded during addition of an aqueous suspension of 0.25 mg/mL RGO (0−25 μL): (a) 0, (b) 0.4 × 10^{-3}, (c) 0.8 × 10^{-3}, (d) 1.2 × 10^{-3}, (e) 1.7 × 10^{-3}, and (f) 2.1 × 10^{-3} mg/mL RGO; λ_{ex} = 440 nm. (B) Decay of the TMPyP fluorescence recorded at different RGO concentrations. Aqueous suspension of 0.25 mg/mL RGO (0−80 μL) was added to 3 mL of 10 μM TMPyP solution in H_2O.

pling between the S_1 and the CT states increases.[68] For TMPyP adsorbed on RGO, we see quenching of the emission with no significant noticeable changes in the shape of the emission band. These results suggest that the singlet excited state of TMPyP interacts with RGO resulting in a weak or nonemissive complex.

In order to probe the excited-state interactions we monitored the emission decay of TMPyP at different RGO concentrations (Figure 2B). The emission of a singlet excited TMPyP monitored in the absence of RGO followed a single exponential decay with a lifetime of 4.9 ns. This value is in good agreement with the literature value reported for the singlet excited state of TMPyP.[67] With increasing concentrations of RGO, we observe an enhanced decay of the excited state, and the decay trace deviates from the single exponential behavior. However, the decay can be fitted with two exponential decay function (for fitting parameters see Table S1 in the Supporting Information). Kinetic parameters obtained during the fitting procedure revealed that short (~1.0 ns) and long (~5.0 ns) time components are the same for all different RGO concentrations. The only difference was that the contribution of the fast components to the overall decay increased with increasing RGO concentration (see pre-exponential factors in Table S1 in the Supporting Information). We attribute the slow and fast components of the emission decay to the excited state of TMPyP in the unbound and the RGO-bound states, respectively. Since free TMPyP and TMPyP adsorbed on RGO exist in equilibrium in the solution, we observe these two components in all the traces.

Binding of TMPyP to RGO Films. The interaction between RGO and TMPyP can also be followed in RGO films cast on glass slides. The strong affinity of TMPyP toward RGO films makes it bind to the RGO film from an aqueous suspension. RGO-coated glass slide was immersed into an aqueous solution containing TMPyP, and the absorption spectrum of the film was recorded at different times. With increasing immersion time, we observe an increase in the absorption with a maximum around 452 nm, thereby confirming the porphyrin binding to RGO film (Figure 3A). This absorption band is red-shifted with respect to the 422 nm absorption maximum of TMPyP in solution and resembles closely the RGO−TMPyP complex presented in Figure 1B.

Initially recorded absorption maximum of the TMPyP on RGO film (after 1 min of immersion of the RGO film in the TMPyP solution) appears at around 452 nm. This absorption maximum corresponds to the one observed

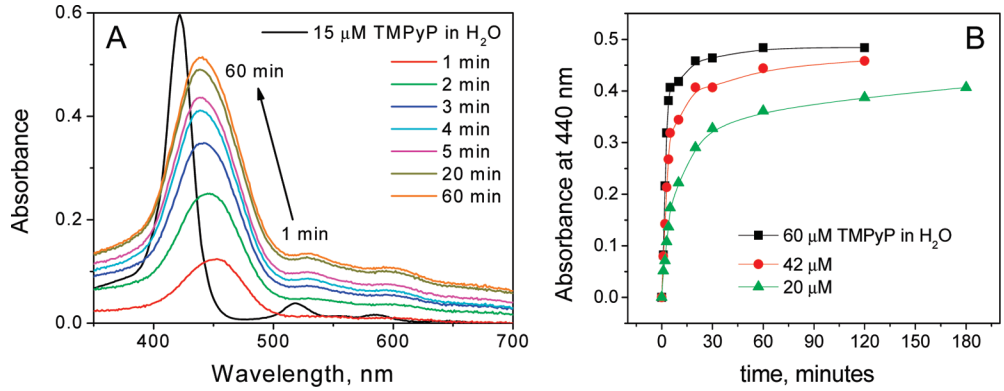

Figure 3. (A) Adsorption of TMPyP on RGO film monitored by UV−vis spectroscopy. FTO plate coated with RGO was immersed in 60 μM aqueous solution of TMPyP, and its absorption spectra were recorded at various immersion times (all corrected for absorption of RGO film itself). (B) Adsorption kinetics of TMPyP on RGO films depending on the concentration of the TMPyP in solution.

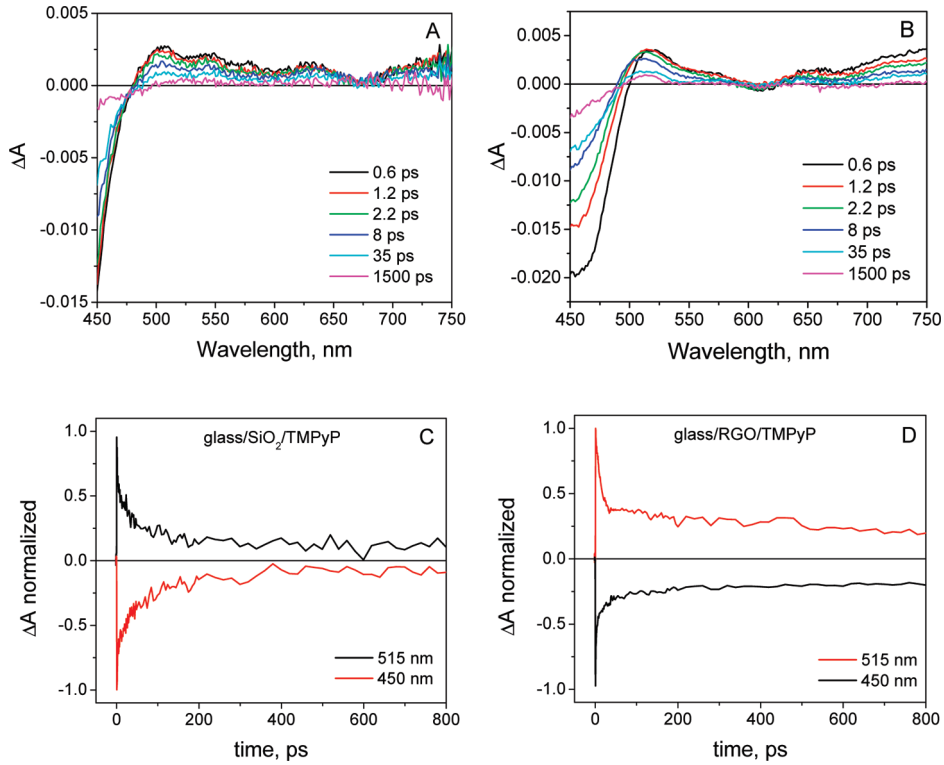

Figure 4. Absorption characteristics of transients obtained following a 387 nm laser pulse excitation of TMPyP-sensitized films. Time-resolved spectra recorded for TMPyP adsorbed on (A) SiO_2 and (B) RGO films. (C) Normalized absorption time profiles taken at 450 and 515 nm for TMPyP adsorbed on SiO_2 and (D) RGO films. Mean laser power during all the experiments: 41 mW/cm^2.

in Figure 1B for the RGO−TMPyP complex. However, it shows a slow blue-shift as an increasing number of TMPyP molecules become attached to the RGO film. After an hour of immersion time, the absorption maximum shifts to 440 nm. It is apparent that as more TMPyP is loaded onto RGO film, the interaction with RGO is influenced by the intermolecular interaction between TMPyP molecules. As shown for mixed Langmuir−Blodgett films with calix[8]arene carboxylic acid derivative, compensation of porphyrin positive charges by carboxylic groups results in self-aggregation of the TMPyP molecules.[69] Although we do not observe any characteristic aggregation bands, the increased loading of TMPyP on RGO seems to have an effect on the interactive properties.

The rate of binding of the TMPyP to the RGO films was monitored by recording the UV−vis absorption spectra of the RGO-coated glass slides at different immersion times in TMPyP solutions. The growth of absorption was followed at 440 nm for three different TMPyP solution concentrations. Figure 3B shows the increase in the absorption at 440 nm *versus* the immersion time for three different sets of experiments. The increase in absorption of the RGO−TMPyP film follows a Langmuir adsorption profile. With increasing TMPyP concentration we observe a faster rate of binding, but they all tend to attain the same saturation level (absorbance at 440 nm 0.45± 0.05). These results further ascertain that the binding of TMPyP is finite, and it is limited by the finite sites available on the RGO film. Based on the change in the absorbance of TMPyP solution, we estimate 2.2×10^{-8} moles of TMPyP per cm^2 of RGO film.

Femtosecond Transient Absorption Spectroscopy of Glass/RGO/TMPyP Films. The porphyrin-sensitized RGO films for transient absorption measurements were prepared by drop-casting RGO suspensions on glass slides and immersing them in TMPyP solution for 2 h. A silica-coated glass slide served as a neutral support to adsorb TMPyP from the solution. These films are referred to as RGO/TMPyP and SiO_2/TMPyP, respectively. RGO/TMPyP films exhibit absorption maximum around 440 nm, whereas SiO_2/TMPyP films shows absorption maximum at 430 nm (Supporting Information, Figure S2). The glass slides were inserted in a spectroscopic cell and evacuated before subjecting them to a 387 nm laser pulse excitation. Time-resolved transient spectra were recorded for the two samples separately (Figure 4A and B). The spectra recorded immediately after the laser pulse excitation exhibited absorption with a maximum around 515 nm, corresponding to the formation of an excited singlet state ^{1}(TMPyP)*. The bleaching of the absorption below 480 nm was the result of ground-state depletion as the TMPyP molecules were excited with the laser pulse.

We also followed the transient absorbance behavior in time at 450 and 515 nm. The initial decay of the ^{1}(TMPyP)* at 515 nm corresponds well with the ground-

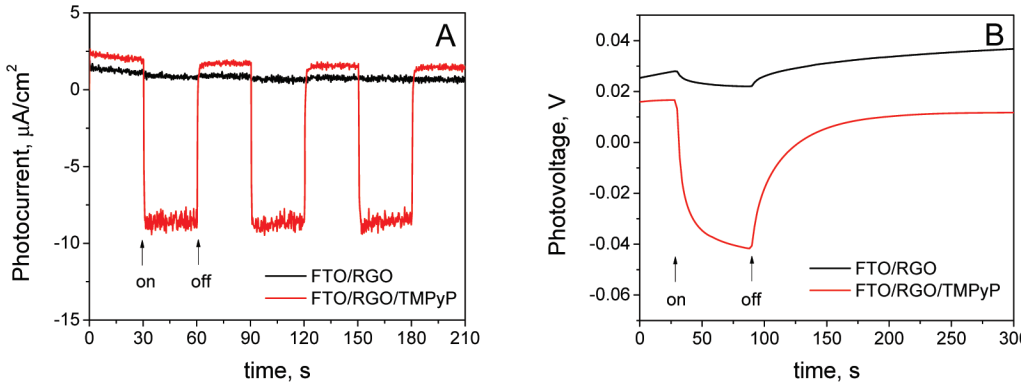

Figure 5. (A) Photocurrent and (B) photovoltage responses of FTO/RGO and FTO/RGO/TMPyP electrodes under white light illumination (λ > 300 nm; input power: 100 mW/cm²; and electrolyte: 0.5 LiI in ACN).

state bleach recovery at 450 nm for both samples (Figure 4C and D). Lifetime of the ^{1}(TMPyP)* was remarkably shorter (<0.25 ns) as compared to the singlet lifetime in solution (4.9 ns). Accelerated decay of the porphyrin excited state is expected in solid films as they undergo deactivation *via* excited-state annihilation processes. Although the transient spectra of SiO_2/TMPyP and RGO/TMPyP films taken immediately after the excitation pulse exhibit similar features, the spectra recorded at 1500 ps time delay shows some difference. The residual absorbance in the case of RGO/TMPyP appears in the traces recorded at 515 and 450 nm (Figure 4D). The presence of a long-lived absorption is indicative of the fact that interaction of ^{1}(TMPyP)* with RGO leads to the formation of a long-lived transient. The appearance of a transient at longer delay times is attributed to the porphyrin radical cation formed during the electron-transfer process (reaction 3):

$$^1(\text{TMPyP})^* + \text{RGO} \rightarrow (\text{TMPyP})^{\bullet+} + \text{RGO(e)} \qquad (3)$$

Based on the earlier reported spectra for the radical cations of ZnTMPyP and NiTMPyP,[70,71] one can postulate that the radical cation exhibits pronounced absorbance below 550 nm. We also employed the nanosecond pulse radiolysis technique to confirm the assignment of absorption band to the cation radical. Bromide radical anions ($Br_2^{\bullet-}$) were used to oxidize the TMPyP molecules, and the radical cation formed during the electron-transfer process was characterized for its absorption features (for details see Supporting Information, Figure S3). Electron injection from the excited singlet TMPyP to RGO film can be ascertained from the estimated oxidation potential of the ^{1}(TMPyP)* (−0.29 V *vs* NHE),[72] which is lower than the reported Fermi level of the RGO (0 V *vs* NHE).[73] Such a difference in the energy levels between donor and acceptor should be sufficient to drive the electron transfer from the photoexcited porphyrin to the RGO.

Photoelectrochemical Measurements with FTO/RGO/TMPyP as Working Electrode. If indeed the excited-state interaction between excited TMPyP and RGO leads to electron transfer, we should be able to probe this effect in a photoelectrochemical cell. The ability of RGO to accept and shuttle electrons has recently been demonstrated for RGO−TiO_2 films.[30,39] When a FTO/RGO/TMPyP electrode was placed in a two-arm photoelectrochemical cell containing 0.5 M LiI in acetonitrile as the electrolyte and irradiated with visible light, we observed anodic photocurrent generation. The magnitude of the photocurrent (~10 μA/cm²) and photovoltage (~60 mV) observed for the FTO/RGO/TMPyP electrode was relatively small compared to other porphyrin−C_{60} or porphyrin−carbon nanotube films.[48,51] However, the fact that we are able to attain anodic photocurrent with these films suggests electron injection from the photoexcited TMPyP to the RGO film (reaction 3). Blank experiments carried out with FTO coated with RGO films produced a negligibly small photoelectrochemical effect under similar experimental conditions. The photocurrent and photovoltage responses of the two electrodes shown in Figure 5 further highlight the importance of the excited-state interaction between porphyrin and RGO in generating a photoelectrochemical effect.

The observed photocurrent with the RGO−TMPyP electrode was prompt, and the response to visible light can be seen during on−off cycles of irradiation (Figure 5A). Low photocurrent density observed in the present experiments is attributed to the inefficient charge separation in the RGO−TMPyP system. Although the excited state of TMPyP is efficiently quenched by graphene, we observe a very low yield of phorphyrin cation radical. The fast recombination of charge carriers limits the net generation of photocurrent. This observation contrasts the behavior of carbon nanotubes and C_{60} which promotes the photoinduced charge separation. For example, the C_{60}−porphyrin[74] and carbon nanotube−porphyrin[75,76] based systems induce better charge separation, and the electrons can be utilized to generate photocurrent more efficiently. The photovoltage response is shown in Figure 5B. The build-up of the photovoltage is rather slow and attains

a steady state in about 100 s. The decay of photovoltage upon stopping the illumination shows the loss of accumulated electrons to the recombination with redox couple. Such losses are commonly seen for the photoelectrochemical cells employing the nanostructured semiconductor films.[77,78]

The iodide ions present in the electrolyte facilitate regeneration of TMPyP molecules (reaction 4):

$$TMPyP^{\bullet+} + I^- \rightarrow TMPyP + I^{\bullet} + (I^-) \rightarrow I_2^{\bullet-} \qquad (4)$$

Such a regenerative mechanism has been established in earlier studies.[48,51]

CONCLUSIONS

A strong interactive affinity between porphyrin and reduced graphene oxide (RGO) exists both in solution as well as in films, and this interaction leads to a red-shift in the porphyrin absorption band. The singlet excited lifetime of the porphyrin bound to RGO is relatively short (<0.25 ns) as it undergoes an energy and electron-transfer process. The formation of the porphyrin cation radical and the photocurrent generation indicate that a fraction of the excitation results in electron transfer. The molecular interaction with RGO is an important phenomenon that can be further exploited to develop energy conversion assemblies or sensing devices.

EXPERIMENTAL SECTION

Materials. All chemicals (reagent grade) were purchased from Aldrich. Graphite powder, synthetic, conducting grade, −325 mesh, and 99.9995% (metals basis) came from Alfa Aesar.

Graphite Oxide Synthesis. Graphite oxide was prepared by a modified Hummers method.[6] Commercially available graphite powder (200 mg) was mixed with sodium nitrate ($NaNO_3$, 200 mg) and sulfuric acid (H_2SO_4, 9.2 mL) and sonicated in an ice bath for 10 min. Subsequently, potassium permanganate ($KMnO_4$, 1.2 g) was added in small portions to the sonicated mixture, not to exceed a temperature of 20 °C. Sonication was stopped, and the flask was removed from the ice bath. The suspension was stirred for 1 h at a temperature of 35 − 40 °C. Water (10 mL) was added to the reaction vessel with stirring, temperature was raised to *ca*. 100 °C, and the suspension was kept at an elevated temperature (80−90 °C) for 20 min. After the addition of 3% hydrogen peroxide (H_2O_2, 60 mL), the suspension was filtered, and the dark-brown precipitate was washed twice with 1 M HCl and with distilled water until the pH of the filtrate was neutral. Graphene oxide was dried in the oven for 24 h at 60 °C and ground in a mortar to obtain a fine dark-brown powder. Stable suspensions of graphene oxide (GO) were obtained by sonicating graphite oxide in water for 1 h. Final concentration of GO in the stock solution used for the reduction was 0.5 mg/mL.

Reduction of Graphene Oxide. Reduced graphene oxide (RGO) was obtained by a chemical reduction of GO (0.5 mg/mL water) with an excess of sodium borohydride (150 mM $NaBH_4$), according to an earlier described procedure.[79] Reaction mixture was kept at an elevated temperature of 80−90 °C for 30 min when the brown suspension turned into black, thus confirming the reduction. Reaction mixture was centrifuged at 10 000 rcf for 15 min to precipitate the reduced graphene oxide, which subsequently was redispersed in water to give concentrations of 0.5 mg/mL based on initial GO concentration.

Preparation of Films. RGO films were prepared by spray coating 0.5 mg/mL RGO aqueous suspensions onto glass slides covered with conducting fluorine-doped tin oxide (FTO) and were employed in photoelectrochemical and TMPyP adsorption measurements after annealing the slides at 100 °C. For transient absorption measurements, RGO suspension was drop casted on to glass slides. The RGO films were modified with porphyrin by immersing the glass slides in 60 μM aqueous solutions of TMPyP for 2 h. TMPyP deposited on SiO_2-coated glass slides (glass/SiO_2/TMPyP) served as controls (blanks) in the femtosecond transient absorption measurements. The SiO_2 films were cast on glass slides by doctor-blading SiO_2 paste (mixture of colloidal SiO_2 and polyethylene glycol PEG) and by subsequent annealing for 1 h at 450 °C. These slides were then immersed in 60 μM aqueous solutions of TMPyP for 2 h.

Methods. All experiments were carried out at room temperature (298 K). Absorption spectra were measured with Varian Cary 50-Bio UV−vis spectrophotometer or double beam Shimadzu UV-3101PC spectrophotometer. Fluorescence spectra were recorded using Horiba Yobin Ivon spectrophotometer, with the use of an appropriate long pass filter to eliminate scattered light from the excitation source. Atomic force microscopy (AFM) images were recorded using Veeco BioScope II with phosphorus n-doped silicon tip under tapping mode. Films for AFM images were obtained by drop-casting diluted GO and RGO solutions onto freshly cleaved mica.

Time-Correlated Single Photon Counting (TCSPC). Emission lifetimes were measured using the Horiba Jobin Yvon DataStation HUB operating in time-correlated single photon counting mode (TCSPC). NanoLED diode emitting pulses at 457 nm with 1 MHz repetition rate and pulse duration of 1.3 ns was used as an excitation source. Light-scattering Ludox solution (colloidal silica) was used to obtain the instrument response function (prompt). For all the measured samples, a long pass 500 nm filter was placed before the emission monochromator. Horiba Jobin Yvon DAS6 fluorescence decay analysis software was used to fit the model functions (one- and two-exponential decays) to the experimental data, with appropriate correction for the instrument response.

Femtosecond Transient Absorption Spectroscopy. Femtosecond transient absorption experiments were conducted using a CPA-2010 1 kHz amplified Ti:sapphire laser system from Clark MXR, combined with a Helios optical detection system provided by Ultrafast Systems. The fundamental output of the CPA-2010 laser system (775 nm, 1 mJ per pulse, and pulse width 150 fs) was split into two beams: a pump (95%) and a probe (5%). The pump beam was directed through a second harmonic generator to provide a 387 nm excitation wavelength used in all the experiments. The probe beam passed through an optical delay rail, allowing regulation of an appropriate delay time between the pump and the probe. Transient absorption measurements of all films were conducted in evacuated spectroscopic cells.

Photoelectrochemical Measurements. Photoelectrochemical measurements were carried out in a two-armed cell consisting of working and platinum-gauze counter electrodes using a Princeton Applied Research potentiostat PARSTAT 2263. Acetonitrile solution containing 0.5 M LiI was used as a redox couple/electrolyte (purged with nitrogen for 10 min prior to each measurement). A 150 W xenon lamp with $CuSO_4/H_2O$ filter was used as a white-light source.

Acknowledgment. The financial support of the Department of Energy, Office of Basic Energy Sciences is gratefully acknowledged. This is contribution number NDRL-4865 from the Notre Dame Radiation Laboratory.

Supporting Information Available: AFM images of GO and RGO, fitting parameters for the fluorescence decays, absorption spectra of films used in the femtosecond transient absorption measurements, and spectra of the TMPyP radical cation obtained by pulse radiolysis are presented. This material is available free of charge *via* the Internet at http://pubs.acs.org.

REFERENCES AND NOTES

1. Rao, C. N. R.; Sood, A. K.; Voggu, R.; Subrahmanyam, K. S. Some Novel Attributes of Graphene. *J. Phys. Chem. Lett.* **2010**, *1*, 572–580.
2. Rao, C. N. R.; Sood, A. K.; Subrahmanyam, K. S.; Govindaraj, A. Graphene: The New Two-Dimensional Nanomaterial. *Angew. Chem., Int. Ed.* **2009**, *48*, 7752–7777.
3. Novoselov, K. S.; Geim, A. K.; Morozov, S. V.; Jiang, D.; Zhang, Y.; Dubonos, S. V.; Grigorieva, I. V.; Firsov, A. A. Electric Field Effect in Atomically Thin Carbon Films. *Science* **2004**, *306*, 666–669.
4. Kamat, P. V. Graphene-Based Nanoarchitectures. Anchoring Semiconductor and Metal Nanoparticles on a Two-Dimensional Carbon Support. *J. Phys. Chem. Lett.* **2010**, *1*, 520–527.
5. Li, L.-S.; Yan, X. Colloidal Graphene Quantum Dots. *J. Phys. Chem. Lett.* **2010**, *257*, 2–2576.
6. Hummers, W. S.; Offeman, R. E. Preparation of Graphitic Oxide. *J. Am. Chem. Soc.* **1958**, *80*, 1339.
7. Li, D.; Muller, M. B.; Gilje, S.; Kaner, R. B.; Wallace, G. G. Processable Aqueous Dispersions of Graphene Nanosheets. *Nat. Nanotechnol.* **2008**, *3*, 101–105.
8. Guo, H. L.; Wang, X. F.; Qian, Q. Y.; Wang, F. B.; Xia, X. H. A Green Approach to the Synthesis of Graphene Nanosheets. *ACS Nano* **2009**, *3*, 2653–2659.
9. Dreyer, D. R.; Park, S.; Bielawski, C. W.; Ruoff, R. S. The Chemistry of Graphene Oxide. *Chem. Soc. Rev.* , *39*, 228–240.
10. Park, S.; Ruoff, R. S. Chemical Methods for the Production of Graphenes. *Nat. Nanotechnol.* **2009**, *4*, 217–224.
11. Seger, B.; Kamat, P. V. Electrocatalytically Active Graphene-Platinum Nanocomposites. Role of 2-D Carbon Support in PEM Fuel Cells. *J. Phys. Chem. C* **2009**, *113*, 7990–7995.
12. Vinodgopal, K.; Neppolian, B.; Lightcap, I. V.; Grieser, F.; Ashokkumar, M.; Kamat, P. V. Sonolytic Design of Graphene Au Nanocomposites. Simultaneous and Sequential Reduction of Graphene Oxide and Au(III). *J. Phys. Chem. Lett.* **2010**, 1987–1993.
13. Jasuja, K.; Linn, J.; Melton, S.; Berry, V. Uncapped Catalytically-enhanced, Solution-dispersed Graphene supported Metal Nanoparticles Grown via Microwave Reduction: Tuning Catalytic, Electrical and Raman Properties. *J. Phys. Chem. Lett.* **2010**, *1*, 1853–1860.
14. Hassan, H. M. A.; Abdelsayed, V.; Khder, A. E. R. S.; AbouZeid, K. M.; Terner, J.; El-Shall, M. S.; Al-Resayes, S. I.; El-Azhary, A. A. Microwave synthesis of graphene sheets supporting metal nanocrystals in aqueous and organic media. *J. Mater. Chem.* **2009**, *19*, 3832–3837.
15. Abdelsayed, V.; Moussa, S.; Hassan, H. M.; Aluri, H. S.; Collinson, M. M.; El-Shall, M. S. Photothermal Deoxygenation of Graphite Oxide with Laser Excitation in Solution and Graphene-Aided Increase in Water Temperature. *J. Phys. Chem. Lett.* **2010**, *1*, 2804–2809.
16. Williams, G.; Seger, B.; Kamat, P. V. TiO_2-Graphene Nanocomposites. UV-Assisted Photocatalytic Reduction of Graphene Oxide. *ACS Nano* **2008**, *2*, 1487–1491.
17. Williams, G.; Kamat, P. V. Graphene-Semiconductor Nanocomposites. Excited State Interactions between ZnO Nanoparticles and Graphene Oxide. *Langmuir* **2009**, *25*, 13869–13873.
18. Ng, Y. H.; Iwase, A.; Kudo, A.; Amal, R. Reducing Graphene Oxide on a Visible-Light $BiVO_4$ Photocatalyst for an Enhanced Photoelectrochemical Water Splitting. *J. Phys. Chem. Lett.* **2010**, *1*, 2607–2612.
19. An, S. J.; Zhu, Y.; Lee, S. H.; Stoller, M. D.; Emilsson, T.; Park, S.; Velamakanni, A.; An, J.; Ruoff, R. S. Thin Film Fabrication and Simultaneous Anodic Reduction of Deposited Graphene Oxide Platelets by Electrophoretic Deposition. *J. Phys. Chem. Lett.* **2010**, *1*, 1259–1263.
20. Luo, Z. T.; Vora, P. M.; Mele, E. J.; Johnson, A. T. C.; Kikkawa, J. M. Photoluminescence and Band Gap Modulation in Graphene Oxide. *Appl. Phys. Lett.* **2009**, *94*, 111909.
21. Mattevi, C.; Eda, G.; Agnoli, S.; Miller, S.; Mkhoyan, K. A.; Celik, O.; Mostrogiovanni, D.; Granozzi, G.; Garfunkel, E.; Chhowalla, M. Evolution of Electrical, Chemical, and Structural Properties of Transparent and Conducting Chemically Derived Graphene Thin Films. *Adv. Funct. Mater.* **2009**, *19*, 2577–2583.
22. Eda, G.; Mattevi, C.; Yamaguchi, H.; Kim, H.; Chhowalla, M. Insulator to Semimetal Transition in Graphene Oxide. *J. Phys. Chem. C* **2009**, *113*, 15768–15771.
23. Jeong, H. K.; Jin, M. H.; So, K. P.; Lim, S. C.; Lee, Y. H. Tailoring the Characteristics of Graphite Oxides by Different Oxidation Times. *J. Phys. D: Appl. Phys.* **2009**, *42*, 065418.
24. Watcharotone, S.; Dikin, D. A.; Stankovich, S.; Piner, R.; Jung, I.; Dommett, G. H. B.; Evmenenko, G.; Wu, S. E.; Chen, S. F.; Liu, C. P.; Nguyen, S. T.; Ruoff, R. S. Graphene-Silica Composite Thin Films as Transparent Conductors. *Nano Lett.* **2007**, *7*, 1888–1892.
25. Stankovich, S.; Dikin, D. A.; Dommett, G. H. B.; Kohlhaas, K. M.; Zimney, E. J.; Stach, E. A.; Piner, R. D.; Nguyen, S. T.; Ruoff, R. S. Graphene-Based Composite Materials. *Nature* **2006**, *442*, 282–286.
26. Berger, C.; Song, Z.; Li, T.; Li, X.; Ogbazghi, A. Y.; Feng, R.; Dai, Z.; Marchenkov, A. N.; Conrad, E. H.; First, P. N.; de Heer, W. A. Ultrathin Epitaxial Graphite: 2D Electron Gas Properties and a Route toward Graphene-based Nanoelectronics. *J. Phys. Chem. B* **2004**, *108*, 19912–19916.
27. Yang, W.; Ratinac, K.; Ringer, S.; Thordarson, P.; Gooding, J.; Braet, F. Carbon Nanomaterials in Biosensors: Should You Use Nanotubes or Graphene. *Angew. Chem., Int. Ed.* **2010**, *49*, 2114–2138.
28. Dua, V.; Surwade, S. P.; Ammu, S.; Agnihotra, S. R.; Jain, S.; Roberts, K. E.; Park, S.; Ruoff, R. S.; Manohar, S. K. All-Organic Vapor Sensor Using Inkjet-Printed Reduced Graphene Oxide. *Angew. Chem., Int. Ed.* **2010**, *49*, 2154–2157.
29. Ang, P. K.; Chen, W.; Wee, A. T. S.; Loh, K. P. Solution-Gated Epitaxial Graphene as pH Sensor. *J. Am. Chem. Soc.* **2008**, *130*, 14392.
30. Lightcap, I. V.; Kosel, T. H.; Kamat, P. V. Anchoring Semiconductor and Metal Nanoparticles on a Two-Dimensional Catalyst Mat. Storing and Shuttling Electrons with Reduced Graphene Oxide. *Nano Lett.* **2010**, *10*, 577–583.
31. Kou, R.; Shao, Y.; Wang, D.; Engelhard, M. H.; Kwak, J. H.; Wang, J.; Viswanathan, V. V.; Wang, C.; Lin, Y.; Wang, Y.; Aksay, I. A.; Liu, J. Enhanced Activity and Stability of Pt Catalysts on Functionalized Graphene Sheets for Electrocatalytic Oxygen Reduction. *Electrochem. Commun.* **2009**, *11*, 954–957.
32. Liu, Z. F.; Liu, Q.; Huang, Y.; Ma, Y. F.; Yin, S. G.; Zhang, X. Y.; Sun, W.; Chen, Y. S. Organic Photovoltaic Devices Based on a Novel Acceptor Material: Graphene. *Adv. Mater.* **2008**, *20*, 3924.
33. Liu, Q.; Liu, Z. F.; Zhong, X. Y.; Yang, L. Y.; Zhang, N.; Pan, G. L.; Yin, S. G.; Chen, Y.; Wei, J. Polymer Photovoltaic Cells Based on Solution-Processable Graphene and P3HT. *Adv. Funct. Mater.* **2009**, *19*, 894–904.
34. Tang, Y.-B.; Lee, C.-S.; Xu, J.; Liu, Z.-T.; Chen, Z.-H.; He, Z.; Cao, Y.-L.; Yuan, G.; Song, H.; Chen, L.; Luo, L.; Cheng, H.-M.; Zhang, W.-J.; Bello, I.; Lee, S.-T. Incorporation of Graphenes in Nanostructured TiO_2 Films via Molecular Grafting for Dye-Sensitized Solar Cell Application. *ACS Nano* **2010**, *4*, 3482.
35. He, Q.; Sudibya, H. G.; Yin, Z.; Wu, S.; Li, H.; Boey, F.; Huang, W.; Chen, P.; Zhang, H. Centimeter-Long and Large-Scale Micropatterns of Reduced Graphene Oxide Films: Fabrication and Sensing Applications. *ACS Nano* **2010**, *4*, 3201.
36. Ohno, Y.; Maehashi, K.; Yamashiro, Y.; Matsumoto, K. Electrolyte-Gated Graphene Field-Effect Transistors for Detecting pH and Protein Adsorption. *Nano Lett.* **2009**, *9*, 3318–3322.
37. Wen, Y. Q.; Xing, F. F.; He, S. J.; Song, S. P.; Wang, L. H.; Long, Y. T.; Li, D.; Fan, C. H. A graphene-Based Fluorescent Nanoprobe for Silver(I) Ions Detection by Using Graphene

Oxide and a Silver-Specific Oligonucleotide. *Chem. Commun.* **2010**, *46*, 2596–2598.
38. Robinson, J. T.; Perkins, F. K.; Snow, E. S.; Wei, Z.; Sheehan, P. E. Reduced Graphene Oxide Molecular Sensors. *Nano Lett.* **2008**, *8*, 3137–3140.
39. Ng, Y. H.; Lightcap, I. V.; Goodwin, K.; Matsumura, M.; Kamat, P. V. To What Extent Do Graphene Scaffolds Improve the Photovoltaic and Photocatalytic Response of TiO_2 Nanostructured Films. *J. Phys. Chem. Lett.* **2010**, *1*, 2222–2227.
40. Das, B.; Voggu, R.; Rout, C. S.; Rao, C. N. R. Changes in the Electronic Structure and Properties of Graphene Induced by Molecular Charge-Transfer. *Chem. Commun.* **2008**, 5155–5157.
41. Liu, H.; Gao, J.; Xue, M.; Zhu, N.; Zhang, M.; Cao, T. Processing of Graphene for Electrochemical Application: Noncovalently Functionalize Graphene Sheets with Water-Soluble Electroactive Methylene Green. *Langmuir* **2009**, *25*, 12006–12010.
42. Xu, Y.; Bai, H.; Lu, G.; Li, C.; Shi, G. Flexible Graphene Films via the Filtration of Water-Soluble Noncovalent Functionalized Graphene Sheets. *J. Am. Chem. Soc.* **2008**, *130*, 5856–5857.
43. Geng, J.; Jung, H.-T. Porphyrin Functionalized Graphene Sheets in Aqueous Suspensions: From the Preparation of Graphene Sheets to Highly Conductive Graphene Films. *J. Phys. Chem. C* **2010**, *114*, 8227.
44. Xie, L. M.; Ling, X.; Fang, Y.; Zhang, J.; Liu, Z. F. Graphene as a Substrate To Suppress Fluorescence in Resonance Raman Spectroscopy. *J. Am. Chem. Soc.* **2009**, *131*, 9890.
45. Ling, X.; Xie, L.; Fang, Y.; Xu, H.; Zhang, H.; Kong, J.; Dresselhaus, M. S.; Zhang, J.; Liu, Z. Can Graphene be used as a Substrate for Raman Enhancement. *Nano Lett.* **2009**, *10*, 553.
46. Treossi, E.; Melucci, M.; Liscio, A.; Gazzano, M.; Samori, P.; Palermo, V. High-Contrast Visualization of Graphene Oxide on Dye-Sensitized Glass, Quartz, and Silicon by Fluorescence Quenching. *J. Am. Chem. Soc.* **2009**, *131*, 15576–15577.
47. Sandanayaka, A. S. D.; Chitta, R.; Subbaiyan, N. K.; D'Souza, L.; Ito, O.; D'Souza, F. Photoinduced Charge Separation in Ion-Paired Porphyrin-Single-Wall Carbon Nanotube Donor-Acceptor Hybrids. *J. Phys. Chem. C* **2009**, *113*, 13425–13432.
48. Hasobe, T.; Fukuzumi, S.; Kamat, P. V. Organized Assemblies of Single Wall Carbon Nanotubes and Porphyrin for Photochemical Solar Cells: Charge Injection from Excited Porphyrin into Single-Walled Carbon Nanotubes. *J. Phys. Chem. B* **2006**, *110*, 25477–25484.
49. Baskaran, D.; Mays, J. W.; Zhang, X. P.; Bratcher, M. S. Carbon Nanotubes with Covalently Linked Porphyrin Antennae: Photoinduced Electron Transfer. *J. Am. Chem. Soc.* **2005**, *127*, 6916–6917.
50. Campidelli, S.; Sooambar, C.; Diz, E. L.; Ehli, C.; Guldi, D. M.; Prato, M. Dendrimer-Functionalized Single-Wall Carbon Nanotubes: Synthesis, Characterization, and Photoinduced Electron Transfer. *J. Am. Chem. Soc.* **2006**, *128*, 12544–12552.
51. Hasobe, T.; Imahori, H.; Fukuzumi, S.; Kamat, P. V. Light Energy Conversion Using Mixed Molecular Nanoclusters. Porphyrin and C-60 Cluster Films for Efficient Photocurrent Generation. *J. Phys. Chem. B* **2003**, *107*, 12105–12112.
52. Hasobe, T.; Kamat, P. V.; Troiani, V.; Solladie, N.; Ahn, T. K.; Kim, S. K.; Kim, D.; Kongkanand, A.; Kuwabata, S.; Fukuzumi, S. Enhancement of Light-Energy Conversion Efficiency by Multi-Porphyrin Arrays of Porphyrin-Peptide Oligomers with Fullerene Clusters. *J. Phys. Chem. B* **2005**, *109*, 19–23.
53. Nakamura, T.; Ikemoto, J.; Fujitsuka, M.; Araki, Y.; Ito, O.; Takimiya, K.; Aso, Y.; Otsubo, T. Control of Photoinduced Energy- and Electron-Transfer Steps in Zinc Porphyrin-Oligothiophene-Fullerene Linked Triads with Solvent Polarity. *J. Phys. Chem. B* **2005**, *109*, 14365–14374.
54. Imahori, H.; Ueda, M.; Kang, S.; Hayashi, H.; Hayashi, S.; Kaji, H.; Seki, S.; Saeki, A.; Tagawa, S.; Umeyama, T.; Matano, Y.; Yoshida, K.; Isoda, S.; Shiro, M.; Tkachenko, N. V.; Lemmetyinen, H. Effects of Porphyrin Substituents on Film Structure and Photoelectrochemical Properties of Porphyrin/Fullerene Composite Clusters Electrophoretically Deposited on Nanostructured SnO_2 Electrodes. *Chem.—Eur. J.* **2007**, *13*, 10182–10193.
55. Xu, Y. F.; Liu, Z. B.; Zhang, X. L.; Wang, Y.; Tian, J. G.; Huang, Y.; Ma, Y. F.; Zhang, X. Y.; Chen, Y. S. A Graphene Hybrid Material Covalently Functionalized with Porphyrin: Synthesis and Optical Limiting Property. *Adv. Mater.* **2009**, *21*, 1275.
56. Gomez-Navarro, C.; Weitz, R. T.; Bittner, A. M.; Scolari, M.; Mews, A.; Burghard, M.; Kern, K. Electronic Transport Properties of Individual Chemically Reduced Graphene Oxide Sheets. *Nano Lett.* **2007**, *7*, 3499–3503.
57. Li, X. L.; Zhang, G. Y.; Bai, X. D.; Sun, X. M.; Wang, X. R.; Wang, E.; Dai, H. J. Highly Conducting Graphene Sheets and Langmuir-Blodgett Films. *Nat. Nanotechnol.* **2008**, *3*, 538–542.
58. Hasobe, T.; Fukuzumi, S.; Kamat, P. V. Ordered Assembly of Protonated Porphyrin Driven by Single-Wall Carbon Nanotubes. J- and H-Aggregates to Nanorods. *J. Am. Chem. Soc.* **2005**, *127*, 11884–11885.
59. Hu, C. G.; Chen, Z. L.; Shen, A. G.; Shen, X. C.; Li, H.; Hu, S. S. Water-Soluble Single-Walled Carbon Nanotubes via Noncovalent Functionalization by a Rigid, Planar and Conjugated Diazo Dye. *Carbon* **2006**, *44*, 428–434.
60. Pasterna, R. F.; Centuro, G. C.; Boyd, P.; Hinds, L. D.; Huber, P. R.; Francesc., L.; Fasella, P.; Engasser, G.; Gibbs, E. Aggregation of Meso-Substituted Water-Soluble Porphyrins. *J. Am. Chem. Soc.* **1972**, *94*, 4511.
61. Xu, Y.; Zhao, L.; Bai, H.; Hong, W.; Li, C.; Shi, G. Chemically Converted Graphene Induced Molecular Flattening of 5,10,15,20-Tetrakis(1-methyl-4-pyridinio)porphyrin and Its Application for Optical Detection of Cadmium(II) Ions. *J. Am. Chem. Soc.* **2009**, *131*, 13490–13497.
62. Chernia, Z.; Gill, D. Flattening of TMPyP Adsorbed on Laponite. Evidence in Observed and Calculated UV-vis Spectra. *Langmuir* **1999**, *15*, 1625–1633.
63. Yao, H.; Kobayashi, S.; Kimura, K. Proof of Partial Flattening of Meso Substituents in Tetracationic Porphyrin at a Mica/Solution Interface. *Chem. Lett.* **2008**, *37*, 594–595.
64. Kuykendall, V. G.; Thomas, J. K. Photophysical Investigation of the Degree of Dispersion of Aqueous Colloidal Clay. *Langmuir* **1990**, *6*, 1350–1356.
65. Ceklovský, A.; Czímerová, A.; Lang, K.; Bujdák, J. Effect of the Layer Charge on the Interaction of Porphyrin Dyes in Layered Silicates Dispersions. *J. Lumin.* **2009**, *129*, 912–918.
66. Benesi, H. A.; Hildebrand, J. H. A Spectrophotometric Investigation of the Interaction of Iodine with Aromatic Hydrocarbons. *J. Am. Chem. Soc.* **1949**, *71*, 2703–2707.
67. Kalyanasundaram, K. Photochemistry of Water-Soluble Porphyrins: Comparative Study of Isomeric Tetrapyridyl- and Tetrakis(N-methylpyridiniumyl)Porphyrins. *Inorg. Chem.* **1984**, *23*, 2453–2459.
68. Vergeldt, F. J.; Koehorst, R. B. M.; van Hoek, A.; Schaafsma, T. J. Intramolecular Interactions in the Ground and Excited States of Tetrakis(N-methylpyridyl)porphyrins. *J. Phys. Chem.* **1995**, *99*, 4397–4405.
69. de Miguel, G.; Perez-Morales, M.; Martin-Romero, M. T.; Munoz, E.; Richardson, T. H.; Camacho, L. J-Aggregation of a Water-Soluble Tetracationic Porphyrin in Mixed LB Films with a Calix[8]arene Carboxylic Acid Derivative. *Langmuir* **2007**, *23*, 3794–3801.
70. Neta, P. One-Electron Transfer Reactions Involving Zinc and Cobalt Porphyrins in Aqueous Solutions. *J. Phys. Chem.* **1981**, *85*, 3678–3684.
71. Nahor, G. S.; Neta, P.; Hambright, P.; Robinson, L. R. One-Electron Oxidation of Nickel Porphyrins: Effect of Structure and Medium on Formation of Nickel(III) Porphyrin or Nickel(II) Porphyrin Pi-Radical Cation. *J. Phys. Chem.* **1991**, *95*, 4415–4418.

72. Kalyanasundaram, K.; Neumann-Spallart, M. Photophysical and Redox Properties of Water-Soluble Porphyrins in Aqueous Media. *J. Phys. Chem.* **1982**, *86*, 5163–5169.
73. Khomyakov, P. A.; Giovannetti, G.; Rusu, P. C.; Brocks, G.; van den Brink, J.; Kelly, P. J. First-Principles Study of the Interaction and Charge Transfer between Graphene and Metals. *Phys. Rev. B: Condens. Matter Mater. Phys.* **2009**, *79*, 195425.
74. Hasobe, T.; Imahori, H.; Fukuzumi, S.; Kamat, P. V. Light Energy Harvesting Using Mixed Molecular Nanoclusters. Porphyrin and C_{60} Cluster Films for Efficient Photocurrent Generation. *J. Phys. Chem. B* **2003**, *107*, 12105–12112.
75. Hasobe, T.; Fukuzumi, S.; Kamat, P. V. Organized Assemblies of Single Wall Carbon Nanotubes and Porphyrin for Photochemical Solar Cells: Charge Injection from Excited Porphyrin into Single-walled Carbon Nanotubes. *J. Phys. Chem. B* **2006**, *110*, 25477–25484.
76. D'Souza, F.; Sandanayaka, A. S. D.; Ito, O. SWNT-Based Supramolecular Nanoarchitectures with Photosensitizing Donor and Acceptor Molecules. *J. Phys. Chem. Lett.* **2010**, *1*, 2586–2593.
77. Thavasi, V.; Renugopalakrishnan, V.; Jose, R.; Ramakrishna, S. Controlled Electron Injection and Transport at Materials Interfaces in Dye Sensitized Solar Cells. *Mater. Sci. Eng., R* **2009**, *63*, 81–99.
78. Gratzel, M. Solar Energy Conversion by Dye-Sensitized Photovoltaic Cells. *Inorg. Chem.* **2005**, *44*, 6841–6851.
79. Shin, H. J.; Kim, K. K.; Benayad, A.; Yoon, S. M.; Park, H. K.; Jung, I. S.; Jin, M. H.; Jeong, H. K.; Kim, J. M.; Choi, J. Y.; Lee, Y. H. Efficient Reduction of Graphite Oxide by Sodium Borohydrilde and Its Effect on Electrical Conductance. *Adv. Funct. Mater.* **2009**, *19*, 1987–1992.